

# Evaluation of nonequilibrium boundary conditions for hypersonic rarefied gas flows

Nam T. P. Le<sup>1</sup>, Christopher J. Greenshields and Jason M. Reese

*Department of Mechanical Engineering, University of Strathclyde, Glasgow G1 1XJ, United Kingdom*

## Abstract

A new CFD solver for high speed viscous flows in the OpenFOAM code is validated against published experimental data and Direct Simulation Monte Carlo (DSMC) results. The laminar flat plate and circular cylinder cases are studied for Mach numbers,  $Ma$ , ranging from 6–12.7, and with argon and nitrogen as working gases. Simulation results for the laminar flat plate cases show that the combination of accommodation coefficient values  $\sigma_u = 0.7$  and  $\sigma_T = 1.0$  in the Maxwell/Smoluchowski conditions, and the coefficient values  $A_1 = 1.5$  and  $A_2 = 1.0$  in the second order velocity slip condition, give best agreement with experimental data of surface pressure. The values  $\sigma_u = 0.7$  and  $\sigma_T = 1.0$  also give good agreement with DSMC data of surface pressure at the stagnation point in the circular cylinder case at  $Kn = 0.25$ . The Langmuir surface adsorption condition is also tested for the laminar flat plate case, but initial results were not as good as the Maxwell/Smoluchowski boundary conditions.

## 1 Introduction

The efficient and accurate simulation of hypersonic rarefied gas flow is important in the aerodynamic design of space vehicles; in particular, predictions of the temperature and pressure experienced by the surface of the vehicle. There are different techniques for simulating these flows, including the DSMC method and CFD. Most successful is the DSMC method, however the computational time required is much longer than for CFD, which generally solves the Navier-Stokes-Fourier (N-S-F) hydrodynamic equations. The translational thermodynamic nonequilibrium of the gas flow can be characterized by the Knudsen number:

$$Kn = \frac{\lambda}{L} \approx \frac{\lambda}{Q} |\nabla Q|, \quad (1)$$

where  $\lambda$  is the mean free path,  $L$  is the macroscopic characteristic length scale, and  $Q$  is a quantity of interest such as the gas temperature, surface and density.

At low altitudes, the gas density is relatively high,  $Kn$  is small, and gas flows may be effectively simulated by solving the Euler equations (when  $Kn \leq 0.001$ ) or the N-S-F equations with no-slip boundary conditions (when  $0.001 \leq Kn \leq 0.01$ ). At high altitude,

---

<sup>1</sup>Email address: nam.le@strath.ac.uk

the gas density is lower, the mean free path,  $\lambda$ , is large, and nonequilibrium behaviour increases. An approach to improve N-S-F predictions in the range ( $0.01 \leq Kn \leq 0.1$ ) is to apply velocity slip and temperature jump boundary conditions at aerodynamic surfaces.

Nonequilibrium velocity slip and temperature jump boundary conditions include those proposed by Maxwell [1], Smoluchowski [2], Myong [3], and “second order” velocity slip conditions [4]. The problem with the Maxwell/S-moluchowski (M/S) boundary conditions, is that the free parameters the tangential momentum,  $\sigma_u$ , and thermal,  $\sigma_T$ , accommodation coefficients, critically affect simulation results. A similar problem with the second order velocity slip boundary condition is the values of the coefficients of the first and second order terms. The Langmuir boundary condition due to Myong [3] overcomes this problem as the velocity slip and temperature jump coefficients are determined through a Langmuir adsorption isotherm model that gives good results for certain rarefied gas microflows.

In this paper, we present two-dimensional (2D) numerical investigations of the velocity slip and temperature jump boundary conditions, in conjunction with the Navier-Stokes-Fourier equations, to propose the best coefficients for hypersonic rarefied gas flow. Our test cases are a circular cylinder in cross-flow at  $Kn = 0.25$  and the laminar sharp-leading-edge flat plate. In the flat plate case the local Knudsen number (i.e. with the  $L$  in equation (1) a running distance from the leading edge) is much larger than the overall Knudsen number (i.e. with the characteristic length being the total streamwise length of the flat plate). For these sharp-leading-edge geometries, our CFD predictions are expected to agree reasonably with the experimental data due to the increased nonequilibrium behaviour near the leading edge. Our simulation results will be compared with DSMC [5] and experimental data for the flat plate case [6, 7]. The flow conditions of the experiments [6, 7], such as freestream temperature,  $T_\infty$ , freestream pressure,  $p_\infty$  and freestream mean free path,  $\lambda_\infty$ , are shown in Table 1.

Table 1: Flow conditions in previous flat-plate experiments

Researcher(s)	$Ma$	$T_\infty$ (K)	$p_\infty$ (Pa)	$\lambda_\infty$ (mm)	$T_w$ (K)	Gas
Becker [6]	12.7	64.5	3.73	0.23	292	Argon
Metcalf <i>et al.</i> [7]	6.1	83.4	2.97	0.35	77	Nitrogen

## 2 Review of nonequilibrium boundary conditions

Most nonequilibrium slip/jump boundary conditions can be expressed in the form:

$$\phi + a\nabla_{\mathbf{n}}(\mathbf{S} \cdot \phi) = \Phi, \quad (2)$$

where  $\phi$  is the variable of interest, e.g. velocity or temperature;  $\nabla_{\mathbf{n}} \equiv \mathbf{n} \cdot \nabla$  is the component of the gradient normal to the boundary surface with  $\mathbf{n}$  being the unit normal vector defined as positive in the direction pointing out of the flow domain;  $a$  is a

coefficient specific to each boundary condition and  $\Phi$  is the limiting value in the case of no slip/jump, e.g. the wall velocity or temperature. The tensor  $\mathbf{S} = \mathbf{I} - \mathbf{nn}$ , where  $\mathbf{I}$  is the identity tensor, removes normal components of any non-scalar field, e.g. velocity, so that slip only occurs in the direction tangential to the surface. The normal gradient can be expressed numerically as

$$\nabla_{\mathbf{n}}\phi = C_{\Delta}(\phi - \phi_i), \quad (3)$$

where the subscript ‘i’ denotes a value in the numerical cell adjacent to the boundary face of the solid surface, and  $C_{\Delta} = 1/|\mathbf{d}|$ , with  $\mathbf{d}$  the distance from the numerical cell centre to the boundary face centre of the solid surface.

Experimental observations show that the gas temperature at the surface is not equal to the surface temperature. This difference is called the “temperature jump” and is driven by the heat flux normal to the surface. The Smoluchowski model [2] for the temperature jump can be written:

$$T + \frac{2 - \sigma_T}{\sigma_T} \frac{2\gamma}{(\gamma + 1) Pr} \lambda \nabla_{\mathbf{n}} T = T_w, \quad (4)$$

where  $\sigma_T$  is the thermal accommodation coefficient  $0 \leq \sigma_T \leq 1.0$ ;  $T$  is the gas temperature at the surface;  $T_w$  is the surface temperature;  $Pr$  is the Prandtl number;  $\gamma$  is the specific heat ratio and  $\lambda$  is the mean free path at the wall. There are a number of different definitions of the mean free path  $\lambda$ ; here we use the Maxwellian

$$\lambda \approx \frac{\mu}{\rho} \sqrt{\frac{\pi}{2RT}}, \quad (5)$$

where  $\rho$  is the gas density at the surface;  $R$  is the specific gas constant;  $\mu$  is the gas viscosity at the surface.

The Maxwell slip boundary condition [1] including the effect of thermal creep, can be written in vector form as:

$$\mathbf{u} = - \left( \frac{2 - \sigma_u}{\sigma_u} \right) \frac{\lambda \boldsymbol{\tau}}{\mu} - \frac{3 Pr (\gamma - 1)}{4 \gamma p} \mathbf{q} + \mathbf{u}_w, \quad (6)$$

where  $\mathbf{u}$  is the velocity; the tangential shear stress is  $\boldsymbol{\tau} = \mathbf{S} \cdot (\mathbf{n} \cdot \boldsymbol{\Pi})$  and the heat flux is  $\mathbf{q} = \mathbf{Q} \cdot \mathbf{S}$  at the surface; with bold type face denoting a vector quantity;  $\boldsymbol{\Pi}$  is the stress tensor at the surface;  $\mathbf{Q}$  is the heat flux vector along the surface;  $p$  is the gas pressure at the surface;  $\mathbf{u}_w$  is the surface velocity. The tangential momentum accommodation coefficient,  $\sigma_u$ , determines the proportion of molecules reflected from the surface specularly ( $1 - \sigma_u$ ) or diffusely ( $\sigma_u$ ), and  $0 \leq \sigma_u \leq 1$ .

Equation (6) can be expressed in the form of equation (2) by substituting  $\boldsymbol{\tau} = \mathbf{S} \cdot (\mathbf{n} \cdot \boldsymbol{\Pi})$  and  $\boldsymbol{\Pi} = \mu \nabla \mathbf{u} + \boldsymbol{\Pi}_{mc}$ , with  $\boldsymbol{\Pi}_{mc} = \mu (\nabla \mathbf{u})^T - (2/3) \mathbf{I} \text{tr}(\nabla \mathbf{u})$  into equation (6),

where the superscript T denotes the transpose, and tr denotes the trace. Noting that  $\mathbf{S} \cdot \nabla_{\mathbf{n}}\phi \equiv \nabla_{\mathbf{n}}(\mathbf{S} \cdot \phi)$  equation (6) becomes:

$$\mathbf{u} + \left( \frac{2 - \sigma_u}{\sigma_u} \right) \lambda \nabla_{\mathbf{n}}(\mathbf{S} \cdot \mathbf{u}) = \mathbf{u}_w - \left( \frac{2 - \sigma_u}{\sigma_u} \right) \frac{\lambda}{\mu} \mathbf{S} \cdot (\mathbf{n} \cdot \mathbf{\Pi}_{mc}) - \frac{3\mu}{4\rho} \frac{\mathbf{S} \cdot \nabla T}{T}. \quad (7)$$

The right hand side contains 3 terms that are associated with (in order): the wall velocity, the so-called curvature effect [13], and thermal creep.

Myong's boundary conditions for velocity slip and temperature jump are based on the Langmuir adsorption isotherm model. Adsorption is the process by which free gas molecules attach to a solid surface, and the boundary conditions are expressed as [3]:

$$\phi = (1 - \alpha)\phi_g + \alpha\phi_w, \quad (8)$$

where the subscript 'g' denotes a reference value in the gas;  $\alpha$  is the fraction of coverage (i.e. occupied surface sites,  $0 \leq \alpha \leq 1$ ) calculated by [3]:

$$\alpha = \frac{\beta p}{1 + \beta p}, \quad (9)$$

where  $\beta$  is an equilibrium constant relating to the surface temperature and a (measured) heat of adsorption  $D_e$  (J/mol) and is calculated as follows:

$$\beta = \frac{A\lambda}{R_u T_w} \exp\left(\frac{D_e}{R_u T_w}\right), \quad (10)$$

where  $R_u$  is the universal gas constant (J/kmol K),  $A$  is the mean area of a site (m<sup>2</sup>/mol) and is either measured or calculated approximately by  $N_A \pi d^2 / 4$  [3] for monatomic and diatomic gases, with  $d$  the molecular diameter and  $N_A$  the Avogadro number.

If  $\phi_g$  is taken as a reference value a mean free path away in the direction normal to the surface, then  $\phi - \phi_g \approx \lambda \nabla_{\mathbf{n}}\phi$ . Equation (8) can therefore be expressed by:

$$\phi + \frac{\lambda}{\beta p} \nabla_{\mathbf{n}}\phi = \phi_w. \quad (11)$$

Expressed this way, the Langmuir boundary condition has the same form as the Maxwell boundary condition without the thermal creep term and the curvature effects, but with  $(2 - \sigma_u)/\sigma_u$  replaced by  $1/\beta p$ . The coefficient for the Langmuir boundary condition is calculated from equation (10), which depends on the values of  $A$  and  $D_e$ , whereas  $\sigma_u$  is the only free parameter in the Maxwell boundary condition.

The second order velocity slip boundary condition for planar surfaces [4] can be expressed as follows:

$$\mathbf{u} + A_1 \lambda \nabla_{\mathbf{n}}(\mathbf{S} \cdot \mathbf{u}) + A_2 \lambda^2 \nabla_{\mathbf{n}}^2(\mathbf{S} \cdot \mathbf{u}) = \mathbf{u}_w, \quad (12)$$

where  $A_1$  and  $A_2$  are slip coefficients for the first and second order terms respectively. Their values are proposed either from theory or from experiment and are still

the subject of much discussion. Equation (12) can be expressed in the general form of equation (2) by substituting  $\nabla_n \mathbf{u} = C_\Delta(\mathbf{u} - \mathbf{u}_i)$  into equation (12):

$$\mathbf{u} + (A_1\lambda + A_2\lambda^2 C_\Delta)\nabla_n(\mathbf{S} \cdot \mathbf{u}) = \mathbf{u}_w + A_2\lambda^2 C_\Delta \nabla_n(\mathbf{S} \cdot \mathbf{u})_i. \quad (13)$$

From equations (4), (7), (11) and (13), the specific coefficients  $a$  for the different models for velocity slip and temperature jump boundary conditions in the general equation (2) are shown in Table 2.

Table 2: Coefficient  $a$  in equation (2) for various slip/jump boundary conditions

Velocity slip	Temperature jump	Coefficient $a$
–	Smoluchowski	$\lambda((2 - \sigma_T)/\sigma_T)(2\gamma/((\gamma + 1)Pr))$
Maxwell	–	$\lambda(2 - \sigma_u)/\sigma_u$
Langmuir	Langmuir	$\lambda/(\beta p)$
Second-order	–	$A_1\lambda + A_2\lambda^2 C_\Delta$

### 3 Numerical implementation and simulation results

In this work we use OpenFOAM, the open source CFD software [8], that uses finite volume (FV) numerics to solve systems of partial differential equations ascribed on any 3-dimensional unstructured mesh of polygonal cells. FV discretisation is based on Gaussian integration and so uses values and normal gradients of fields at cell faces. If the face belongs to a boundary, the face value and gradient required by the discretisation procedure must be obtained from the boundary condition. Various fundamental types of boundary condition are implemented in OpenFOAM including one known as “partial slip” that is a mixture of a fixed value, or Dirichlet, condition and a zero gradient condition — a Neumann condition where the normal gradient is zero. The “mixing” is controlled by a by a fraction coefficient  $\theta$  ( $0 \leq \theta \leq 1$ ) where  $\theta = 0$  for the zero gradient condition and  $\theta = 1$  for fixed value condition. A reference value is also required that is assigned to the fraction of the boundary condition that is fixed value.

For the case of scalar fields, this boundary condition can be used as the basis for any slip/jump boundary condition described by equation 2, by setting

$$\theta = 1 - \frac{aC_\Delta}{1 + aC_\Delta}, \quad (14)$$

and setting the value  $\Phi$  to be the reference value for the fixed value component. For the case of vector fields, the standard partial slip condition was modified to include the tensor  $\mathbf{S}$  so that only the tangential components of the field are “slipped”. In either case, the fraction values,  $\theta$ , for the boundary conditions considered are simply determined by equation (14) with the values of  $a$  from Table 2. The N-S-F equations are implemented and solved numerically in OpenFOAM using a finite volume discretisation and high-resolution central schemes that are described in detail in [9]. These are implemented as the solver `rhoCentralFoam` in OpenFOAM for simulating high speed viscous flows. A calorically perfect gas is considered for all our simulations in the

present study, so  $p = \rho RT$  and  $e = c_v T = (\gamma - 1) RT$ . The Sutherland law is used for modelling the dynamic viscosity in the flat plate case, i.e.

$$\mu = A_S \frac{T^{1.5}}{T + T_S}, \quad (15)$$

where  $A_S$  and  $T_S$  are constants. The coefficient of thermal conductivity is then computed from  $k = c_p \mu / Pr$ . The values  $A_S$ ,  $T_S$ ,  $R$ ,  $\gamma$  and  $Pr$  of the working gases in the flat plate cases are given in Table 3 [10–12].

Table 3: Coefficients for gas transport properties

Gas	$A_S$ (Pa.s $K^{-1/2}$ )	$T_S$ (K)	$R$ ( $m^2 s^{-2} K^{-1}$ )	$\gamma$	$Pr$
Argon	$1.93 \times 10^{-6}$	142	208.1	1.67	0.67
Nitrogen	$1.41 \times 10^{-6}$	111	296.8	1.4	0.71

The power law is used for modelling the viscosity in the cylinder case, in order to compare with DSMC in [5], i.e.

$$\mu = A_P T^s, \quad (16)$$

where  $s = 0.734$  and  $A_P = 0.32 \times 10^{-6}$  (Pa.s  $K^{-s}$ ) are calculated from [5].

### 3.1 Flat plate case setup

Nonequilibrium boundary conditions are applied on the surface of a flat plate for the flow variables ( $T$ ,  $\mathbf{u}$ ). The boundary condition for the pressure  $p$  at the flat plate is zero normal gradient. At the inflow boundary, the freestream conditions are maintained throughout the computational process. At the top boundary and the outflow boundary fluid is allowed to leave the computing region; this condition specifies that the normal gradients of the flow variables ( $p$ ,  $T$ ,  $\mathbf{u}$ ) vanish at these boundaries. At the lower boundary in front of the flat plate, a symmetry condition is applied to all flow variables. A schematic diagram of the boundary conditions applied in the flat plate cases is shown in figure 1. In our flat plate simulations we used a regular rectangular mesh.

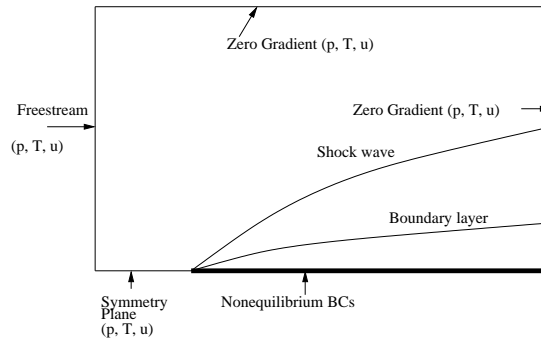


Figure 1: Numerical case setup for the flat plate problem.

The computational results are sensitive to the mesh sizes near the leading edge so we conducted a mesh independence analysis to find the mesh size at which the solution converged. The final mesh sizes were  $\Delta x = 0.1 \lambda_\infty$  and  $\Delta y = 0.1 \lambda_\infty$  for Becker's case, and  $\Delta x = 0.4 \lambda_\infty$  and  $\Delta y = 0.9 \lambda_\infty$  for Metcalf *et al.*'s case.

### 3.2 Circular cylinder case setup

A schematic diagram of the boundary conditions applied in the cylinder case is shown in figure 2(a). The flow conditions for the circular cylinder DSMC case are as fol-

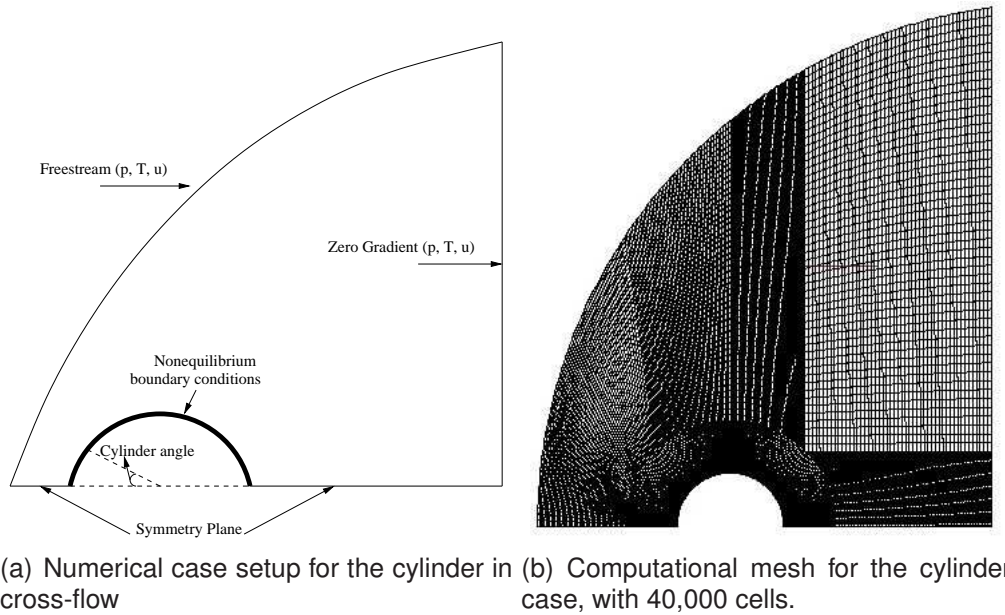


Figure 2: Setup of circular cylinder case.

lows [5]: freestream conditions  $Ma = 10$ ,  $T_\infty = 200$  K,  $p_\infty = 0.05$  Pa, the surface temperature  $T_w = 500$  K, diameter of cylinder  $D = 304.8$  mm,  $Kn = 0.25$  and argon is the working gas. The computational mesh is built to wrap around the leading bow shock. The mesh is graded linearly over the first 100 cells near the surface, so that the mesh size varies from  $10 \mu\text{m} \rightarrow 100 \mu\text{m}$ . The smallest cell size near the surface is  $\Delta x = 10 \mu\text{m}$ ,  $\Delta y = 2.4$  mm, which is approximately the same as the smallest cell size in [5]. A typical mesh of cells for the cylinder simulations is shown in figure 2(b).

## 4 Results

### 4.1 Flat plate experimental cases

For the flat plate case, we carried out three simulations as follows: first using the M/S boundary conditions, second using second order slip velocity and the Smoluchowski temperature jump condition with  $\sigma_T = 1$  (chosen from the results obtained from the first case), and third with no-slip/jump conditions. Different values of the coefficients  $\sigma_u, \sigma_T$  varying from 0.7 to 1 in the M/S boundary conditions, and of  $A_1, A_2$  in the second order velocity slip boundary condition, were employed to attempt to find the best values. Here, the results for surface pressure in the Metcalf *et al.* case [7] are presented versus  $x/\lambda_\infty = Kn^{-1}$  as an illustration.

For the M/S boundary conditions, simulations are run with  $\sigma_u = \sigma_T = 0.7$  and 0.8,

and also  $\sigma_u = 0.7$  and  $\sigma_T = 1.0$ . The combination of values  $\sigma_u = 0.7$  and  $\sigma_T = 1$  give best agreement with the experimental data for  $x/\lambda_\infty \geq 15$  ( $Kn \leq 0.067$ ). There is a large difference between from no-slip/jump results with the experimental data at  $x/\lambda_\infty \leq 40$  ( $Kn \geq 0.025$ ), as seen in figure 3(a). For the second order velocity slip boundary condition, simulations are done with different values of  $A_1, A_2$ , as seen in figure 3(b). The values  $A_1 = 1.5$  and  $A_2 = 1$  give best agreement with the experimental data of the surface pressure. The second order term affects the surface pressure, in that increasing the value of  $A_2$  decreases the pressure.

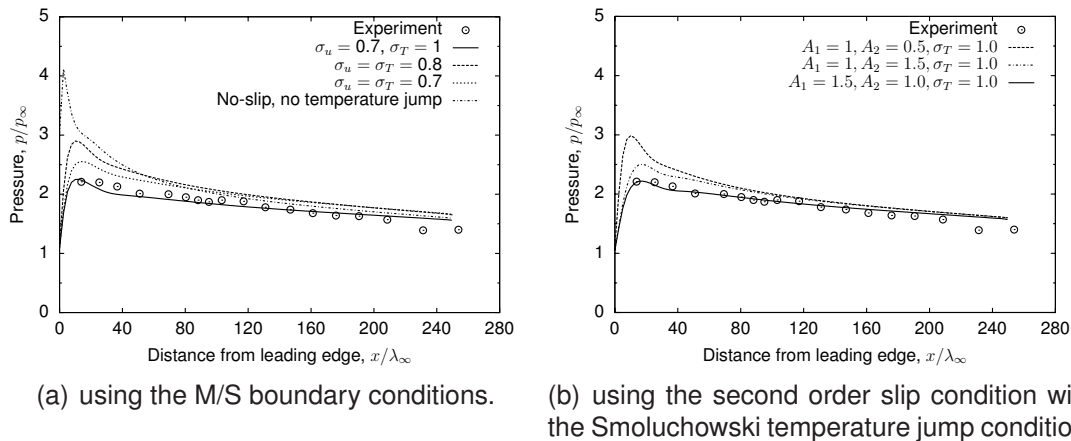


Figure 3: Metcalf *et al.*'s case [7], surface pressure distribution along the flat plate, simulations with the various boundary conditions.

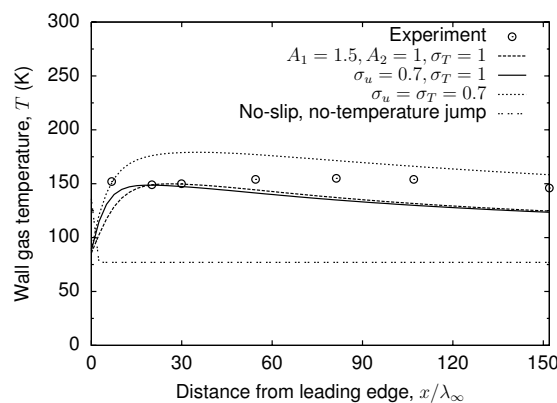
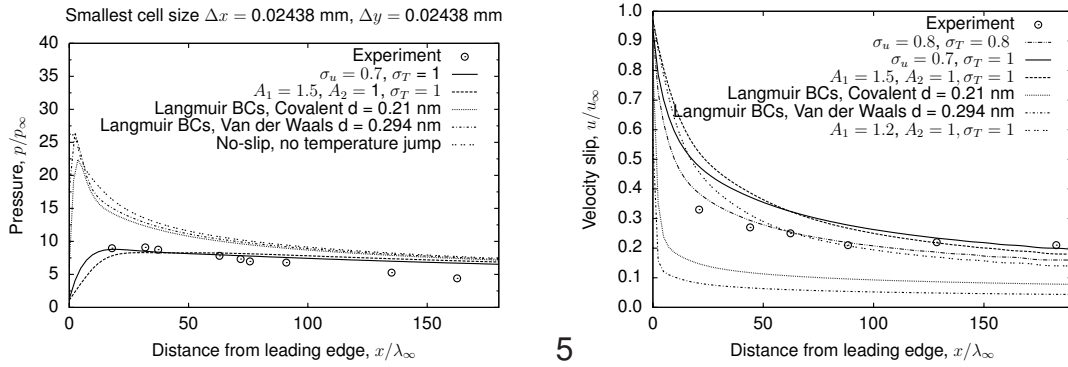


Figure 4: Metcalf *et al.*'s case [7], surface temperature distribution along the flat plate, simulations with the various boundary conditions.

For the surface temperature, the simulations with the M/S boundary conditions with  $\sigma_u = 0.7$  and  $\sigma_T = 1$ , and the second-order slip condition with  $A_1 = 1.5, A_2 = 1$  and the Smoluchowski boundary condition with  $\sigma_T = 1$  give good predictions at the leading edge. The value  $\sigma_T = 1$  is better than the value  $\sigma_T = 0.7$  in predicting the surface temperature at the leading edge. The no-slip/jump results give the surface temperature 77 K along the flat plate, as seen in figure 4.

In the Becker *et al.* case [6], the values  $\sigma_u = 0.7$  and  $\sigma_T = 1$  in the M/S boundary conditions and the values  $A_1 = 1.5$ ,  $A_2 = 1$  in the second order velocity slip boundary condition give best agreement with the experimental data of the surface pressure for  $x/\lambda_\infty \geq 18$  ( $Kn \leq 0.055$ ). There is a large difference between the no-slip/jump results with experimental data at  $x/\lambda_\infty \leq 50$  ( $Kn \geq 0.02$ ), as seen in figure 5(a). For the slip velocity, the values  $\sigma_u = \sigma_T = 0.8$  in the M/S boundary condition give best agreement with the experimental data, as seen in figure 5(b). For the second order slip condition, the values  $A_1 = 1.2$  and  $A_2 = 1$  give good agreement with the experimental data. In this case, we have also applied the Langmuir boundary condition, using in turn both the ‘‘Covalent’’ and the ‘‘Van der Waals’’ diameters  $d$  of the gas molecule. The Covalent diameter is a measure of the size of the molecule which forms part of a covalent bond, and the Van der Waals is the diameter of an imaginary equivalent hard sphere molecule. Our initial results show that the Langmuir model is sensitive to the mean area of a surface site,  $A = N_A \pi d^2 / 4$  [3], and the heat of adsorption  $D_e$ . The results do not give as good agreement with the experimental data as the M/S boundary conditions. More investigations into the appropriate values for  $A$  and  $D_e$  from the experimental literature may be needed to yield better and more reliable results.



(a) Surface pressure distribution along the flat plate, simulations with various boundary conditions. (b) Slip velocity along the flat plate, simulations with various conditions.

Figure 5: Simulation results of Becker’s flat plate case [7].

## 4.2 Circular cylinder DSMC case, $Kn = 0.25$

In the circular cylinder case, we test the coefficient values  $\sigma_u = 0.7$  and  $\sigma_T = 1$  in the M/S conditions, obtained from the flat plate case, with and without the curvature effect i.e. without including the  $\Pi_{mc}$  term in equation (7), and compare with the no-slip/jump results and DSMC data [5].

For the surface pressure, the values  $\sigma_u = 0.7$  and  $\sigma_T = 1$  give good agreement with the DSMC data at the stagnation point ( $\varphi = 0^\circ$ ) while the no-slip/jump case does not. The curvature effect does not strongly affect the surface pressure. There is a difference between DSMC data and our CFD results of simulations with the M/S conditions at

$30^\circ \leq \varphi \leq 180^\circ$ , while the no-slip/jump results agree with DSMC data in this region. For the slip-velocity, simulations with and without the curvature effect disagree with the DSMC data at  $Kn = 0.25$ . The results show that the curvature strongly affects the slip velocity at  $\varphi \geq 60^\circ$ , acting to reduce the peak value of the slip velocity.

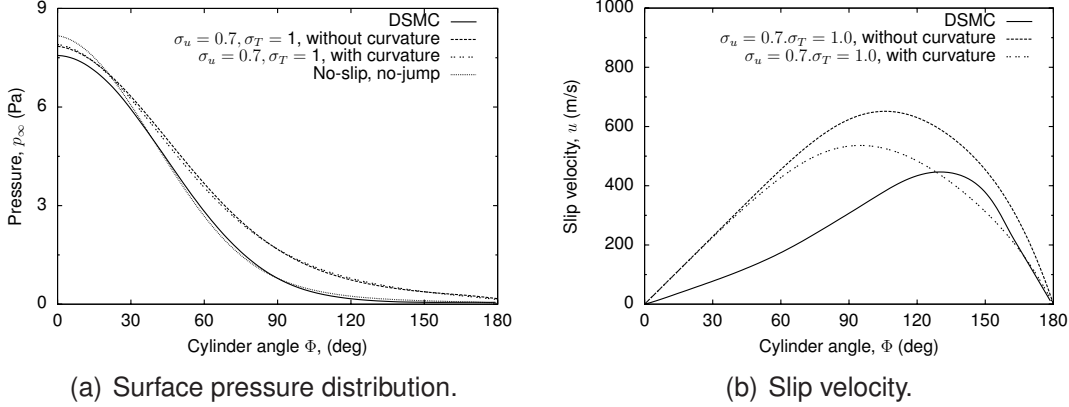


Figure 6: Simulation results of the circular cylinder in cross-flow case.

## 5 Conclusions

Our results show that including velocity slip/temperature jump boundary conditions can improve CFD prediction of high-speed rarefied flows. The values  $\sigma_u = 0.7$ ,  $\sigma_T = 1$  in the M/S boundary conditions, and  $A_1 = 1.5$  and  $A_2 = 1.0$  in the second order slip condition with  $\sigma_T = 1.0$ , give best agreement with the experimental data of the surface pressure up to  $Kn = 0.1$  for the flat plate cases. The values  $\sigma_u = 0.7$  and  $\sigma_T = 1$  also give good agreement with DSMC data of the surface pressure at the stagnation point in the cylinder case.

The Langmuir boundary condition overpredicts the surface pressure and underpredicts the slip-velocity. But the results are sensitive to the values of  $A$  and  $D_e$ , and more appropriate values from experimental literature may improve these results.

From the results obtained in the flat plate case, the N-S-F equations seem to work well with the M/S boundary conditions, or the second order velocity slip and the Smoluchowski boundary conditions, up to  $Kn = 0.1$ . The second order velocity slip boundary condition is not much better than the conventional Maxwell slip boundary condition with the N-S-F model.

The circular cylinder case shows that the N-S-F equations with the M/S boundary conditions did not predict well the slip-velocity at  $Kn = 0.25$ , as compared to DSMC data. This case shows that the curvature effect is important when simulating the slip-velocity in blunt geometries.

## Acknowledgements

N. T. P. L. would like to thank Dr. R. S. Myong and Prof. B. C. Eu for helpful discussions, and the James Weir Foundation and the University of Strathclyde for research scholarships that support this work.

## References

- [1] J. C. Maxwell, On stresses in rarefied gases arising from inequalities of temperature, *Philosophical Transactions of the Royal Society*, Part 1, Vol. 170, pp. 231 – 256, 1879.
- [2] M. von Smoluchowski, Über wärmeleitung in verdünnten gasen, *Annalen der Physik und Chemie*, Vol. 64, pp. 101 - 130, 1898.
- [3] R. S. Myong, Gaseous slip models based on the Langmuir adsorption isotherm, *Physics of Fluids*, Vol. 16, No. 1, pp. 104 – 117, 2004.
- [4] N. G. Hadjiconstantinou, Comment on Cercignani's second order slip coefficient, *Physics of Fluids*, Vol. 15, No. 8, pp. 2352 – 2354, 2003.
- [5] A. J. Lofthouse, Nonequilibrium hypersonic aerothermodynamics using the direct simulation Monte Carlo and Navier-Stokes models, Ph.D. Thesis, University of Michigan, 2008.
- [6] M. Becker, Flat plate flow files and surface measurements from merged layer into transition regime, *Proceedings of the 7th International Symposium on Rarefied Gas Dynamics*, pp. 515 – 528, 1969.
- [7] S. C. Metcalf, D. C. Lillicrap and C. J. Berry, A study of the effect of surface temperature on the shock-layer development over sharp-edge shapes in low-Reynolds-number high-speed flow. *Proceedings of the 7th International Symposium on Rarefied Gas Dynamics*, pp. 619 – 634, 1969.
- [8] [www.openfoam.org](http://www.openfoam.org), 2009.
- [9] C. J. Greenshields, H. G. Weller, L. Gasparini and J. M. Reese, Non-oscillatory central schemes for high speed viscous flows, *accepted by International Journal for Numerical Methods in Fluids*, 2009.
- [10] C. R. Lilley and M. N. Macrossan, DSMC calculations of shock structure with various viscosity laws, *Proceedings of the 23rd International Symposium on Rarefied Gas Dynamics*, pp. 663 – 670, 2002.
- [11] <http://www.imnoeng.com/flow/gasviscosity.htm>, 2008.
- [12] R. C. Weast, CRC Handbook of Chemistry and Physics, *CRC Press Inc*, Florida, USA, 1984.
- [13] D. A. Lockerby, J. M. Reese, D. R. Emerson and R. W. Barber, Velocity boundary condition at solid walls in rarefied gas calculations, *Physical Review E*, Vol. 70, pp. 017303, 2004.